ELSEVIER

Materials Chemistry and Physics 46 (1996) 140–146

MATERIALS CHEMISTRY AND PHYSICS

# Ion implantation into amorphous solids

W.F. van der Weg [a], A.J.M. Berntsen [a], F.W. Saris [b], A. Polman [b]

[a] *Debye Institute, Utrecht University, Utrecht, Netherlands*

[b] *FOM-Institute for Atomic and Molecular Physics, Amsterdam, Netherlands*

Received 21 November 1995; accepted 11 February 1996

**Abstract**

We describe the effects of implantation of silicon into pure amorphous silicon and hydrogenated amorphous silicon and of erbium into soda-lime silicate glass and hydrogenated amorphous silicon. The former implantations and subsequent annealing treatments are used as a means of controlled defect creation. The experiments lead to new insights into the relation between defect density and bond-angle variation in both types of amorphous silicon. Erbium implantation is used to produce planar optical waveguide materials. It is demonstrated that erbium implantation into glass and amorphous silicon leads to efficient photoluminescence. It appears that these materials are attractive candidates for Er-doped waveguide amplifiers.

*Keywords:* Ion implantation; Amorphous solids; Silicon; Erbium implantation

## 1. Introduction

Ion implantation used to modify the mechanical, electrical, or optical properties of surfaces and thin layers has become a ubiquitous technique. Especially the doping of semiconductor crystals by implantation is common in the microelectronics industry. In almost all cases the ion implantation damage has to be annealed out after implantation, in order to restore the crystallinity and electrical properties of the material. Less known, however, is the use of ion implantation to influence the properties of amorphous materials. The reason for this is the common belief that amorphous materials are always defective; ion implantation, in this view, would hardly be expected to modify the properties of such a material.

In this paper we will illustrate the use of ion implantation into various classes of disordered materials with a view to modify the structural and optical properties of such solids. As specific examples we will demonstrate the (self-) implantation of amorphous silicon to modify the concentration of point defects in the material, and the implantation of glasses with optically active rare earth ions.

## 2. Ion implantation of amorphous silicon

Amorphous silicon (a-Si) is a material which is of great interest for a variety of opto-electronic applications. It is widely used in solar cells, in photosensitive layers, in photocopying machines, and in thin film transistors for display purposes. The rapid development of the application of this material in the recent decade stems from the fact that it has been proven possible to dope the material to make n-type or p-type layers. This is only possible when the material is hydrogenated, i.e. when a concentration of the order of 10 at.% H is present in the amorphous silicon layer. Hydrogenated amorphous silicon is commonly designated as a-Si:H.

The optical properties of a-Si:H strongly depend on the details of the structure and hydrogen bonding in the material. We will therefore discuss these properties in more detail in this article.

### 2.1. Structure of amorphous silicon

Amorphous covalent semiconductors, because of the strong directionality of the bonds, in principle, display a short-range order which is very much like the one in crystalline silicon. This means that each atom is fourfold coordinated in a tetrahedral configuration, that the bond length is (to within a few percent) equal to the value in a silicon crystal and that the bond angles are also close to that of the crystalline value (109°). However, while this angle in the crystal is fixed, in a-Si a distribution of angle values exists, with a spread of about 8°. If one measures the radial distribution function, e.g. by neutron scattering, it turns out that not only the first neighbour of a certain central atom can be found at a fixed distance, but also the probability of finding the second nearest neigh-


*PII* S0254-0584(96)01791-9

bour atom strongly peaks at a certain distance. At larger distance the order is lost and this is expressed by stating that there is no long-range order present.

The structure described above is the so-called continuous random network (CRN) and it is associated with ideal amorphous silicon. In practice, the structures obtained with various methods of producing a-Si are far from ideal, in the sense that a large number of threefold coordinations (possibly also five-fold coordinations) occurs, that internal voids with sizes of the order of a few to several tens of (missing) atoms are present and that there is a high concentration of point defects like dangling bonds. These defects are detrimental to the electronic properties of the material and it was therefore a major breakthrough when it was shown that hydrogen atoms can passivate dangling bonds and thereby reduce the density of electronic defect states, making a-Si:H suitable for electro-optical applications.

The detailed structure of the amorphous silicon network is closely related to the method of producing the a-Si and this results in the important realization that amorphous silicon does not have a unique structure. This fact motivates the intense efforts to investigate new ways of producing amorphous silicon with optimized opto-electrical properties.

### 2.2. *Preparation of amorphous silicon*

Initially, a-Si layers were produced by sputtering of a silicon target and depositing the sputtered material on a substrate. This method generally produces amorphous silicon with a rather low density. It contains a high density of internal voids and is not suitable for electronic applications.

The method which is most widely used today, especially in large-scale industrial production, is glow-discharge deposition. In this method, silane gas ($SiH_4$) is introduced into a reactor that has two parallel electrodes. Between the electrodes a radio frequency field (usually with a driving frequency of 13.56 MHz) is applied and this field sets up a discharge in the gas. Electrons produced in this plasma cause partial dissociation of the silane molecules and various hydrogen-containing radicals are deposited on the electrodes. It is generally believed that the $SiH_3$ radical is the most abundant and effective precursor to the growth of the amorphous silicon layer. These layers necessarily contain a high concentration of hydrogen and therefore the glow-discharge, or plasma enhanced CVD (PECVD), method produces a-Si:H material. There is a large range of deposition parameters (like gas flow rate, plasma power, gas pressure, electrode distance, electrode shape), which all influence the material structure. Of these the substrate temperature has the strongest effect on the material properties.

Recently, the method of hot-wire deposition has attracted considerable attention. In this method silane gas is decomposed by a catalytic reaction at a hot (around 2000 °C) tungsten wire. The silane molecules are dissociated at the wire and produce an amorphous silicon layer on a substrate which is situated at a few centimeters' distance from the wire. In this method hydrogen is also introduced in the material. It is interesting that the detailed structure of this material is markedly different from the glow-discharge material. In particular, the hot-wire material appears to exhibit good opto-electronic properties with a far lower hydrogen concentration than the PECVD material.

Finally, amorphous silicon can be produced by high-dose ion implantation in crystalline silicon. In this process, the ion dose exceeds the threshold dose for amorphization of the target. Especially self-implantation (i.e. bombardment with silicon ions) produces a layer of pure, unhydrogenated, amorphous silicon. This type of a-Si generally has a density which is very close to the crystal silicon density and consequently, contains a relatively small number of internal voids. However, this material cannot be used for electrical applications owing to the presence of a large number of electronic defect states associated with the point defects created by the implantation process. Nevertheless, a detailed study of this material and a comparison of its properties with those of a-Si:H has been very helpful in understanding the properties of CRN and particularly in elucidating the role of hydrogen in such structures.

It should be pointed out that in all the methods mentioned for producing a-Si or a-Si:H, only thin layers (roughly up to a micron thick) can be fabricated. This stems from the fact that in the sputtering or plasma deposition process, typical deposition rates are of the order of 1 Å $s^{-1}$. In the implantation amorphization process, very high implantation energies (and doses) are needed to produce an amorphization depth in excess of 1 $\mu$m.

### 2.3. *Analysis techniques*

We will give a short overview of the characterization methods which are used to obtain information about the network and defect structure and the electro-optical properties of amorphous silicon.

#### 2.3.1. *Raman scattering*

The Raman spectrum of crystalline silicon consists of a single sharp peak at an energy of 521 $cm^{-1}$, owing to the interaction of the laser with the transverse optical (TO) vibration mode of the lattice. All other modes are not Raman active, because of the symmetry in the fcc lattice. In contrast, in amorphous silicon, such symmetry does not exist and hence all modes are Raman-active. The peaks in the Raman scattering spectrum also are considerably broadened, compared with the crystal case. It has been shown that, in particular, the width of the TO peak in the spectrum is related to the width of the bond angle distribution in the amorphous network. An example of Raman spectra obtained from a plasma-deposited a-Si:H sample and an ion-beam amorphized sample is presented in Fig. 1.

Fig. 1 enables one to directly draw some important conclusions about the defect production and creation mechanisms in amorphous silicon. Firstly, the bond-angle distri-

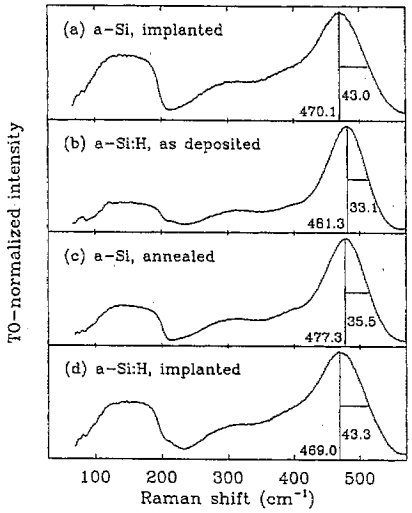


Fig. 1. Raman spectra for (a) a-Si prepared by ion amorphization of c-Si, (b) glow-discharge deposited a-Si:H, (c) ion-implanted a-Si after annealing at 500 °C for 2 h, and (d) a-Si:H after implantation with $3\times10^{15}$ $Si^+$ ions $cm^{-2}$.

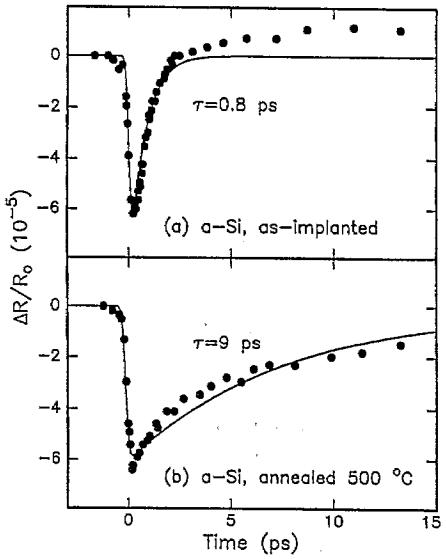


Fig. 2. Normalized changes in reflectivity as a function of the time delay between pump and probe pulse for (a) as-implanted a-Si; (b) a-Si annealed at 500 °C for 1 h.

bution is narrower in a-Si:H. Secondly, its structure is 'better' than that of a-Si in terms of bond angle distribution. Thirdly, the structure of a-Si:H deteriorates upon ion implantation and finally, the network structure improves upon annealing. Apparently, hydrogen addition during the deposition has a beneficial influence on the structure, while ion implantation increases the defect density in the network. Annealing reduces the defect density by a structural relaxation process. However, annealing procedures at moderate temperatures are unable to induce a transition from the amorphous to the crystalline state [1].

### 2.3.2. *Pump-probe reflectivity measurements*

Another estimate of the defect density can be obtained from the lifetime of optically generated free charge carriers in a-Si or a-Si:H. These are excited by a (pump-) laser which excites an electron-hole plasma in the specimen. This density of free charge carriers causes a decrease in the reflectivity of the sample. This reflectivity is probed by a part of the same laser which is incident at a small angle to the surface. This probe laser is time-delayed with respect to the pump and therefore the reflectivity can be measured as a function of time after the pump has been switched off. Because of recombination of carriers at defects in the material, the reflectivity will increase again to its stationary value after a decay. The decay time is related to the defect density in the material. Fig. 2 shows the decay of the reflectivity of implanted and annealed a-Si samples. It can be observed that annealing causes an increase of the carrier lifetime by an order of magnitude. The inverse of the lifetime $\tau$ is linearly dependent on the density of defects in the material [2].

### 2.3.3. *Optical absorption*

Optical reflection and transmission measurements can be used to determine values for the absorption coefficient $\alpha$ above $\sim1.5\times10^3$ $cm^{-1}$. Such data, measured for photon energies between 1.1. and 3.0 eV enables one to calculate the refractive index $n$, the absorption coefficient and the film thickness [3]. For lower values of $\alpha$ the technique of photothermal deflection spectroscopy (PDS) has been applied [4]. In this method, an intensity-modulated light beam is absorbed in a sample, which causes periodic heating. The heat from the absorbing material flows into the surrounding medium causing a modulation of the refractive index. A laser beam grazing the sample surface will thus undergo a periodic deflection, the magnitude of which is proportional to the absorption coefficient of the sample. Thus, if the wavelength of the pump beam is varied, the deflection of the probe monitors the absorption spectrum of the sample.

### 2.3.4. *Infrared spectroscopy*

Hydrogen bonding in the samples is investigated using Fourier-transform infrared absorption spectroscopy. The characteristic absorption frequencies are representative for hydrogen configurations in Si-H, $Si-H_2$, $(Si-H_2)_n$, and $Si-H_3$ groups [5].

## 2.4. *Ion Implantation and Annealing of a-Si and a-Si:H*

The effects of ion implantation and annealing on the optical absorption spectra of a-Si and a-Si:H are quite pronounced. In Fig. 3 absorption spectra for a-Si:H after deposition, after irradiation with various doses, and annealing are presented. The shoulder in the absorption spectrum for $\alpha\leq5$ $cm^{-1}$ (region A) is caused by optical transitions involving defect states, the exponential increase of $\alpha$ from 5 $cm^{-1}$ to $10^3$ $cm^{-1}$ (region B) is dominated by transitions from the valence band tail to the conduction band, while interband transitions are prominent in the regime of $\alpha\geq10^4$ $cm^{-1}$ (region C). The solid lines in Fig. 3 are fits to the measured data obtained with a model for the density of states which was proposed by

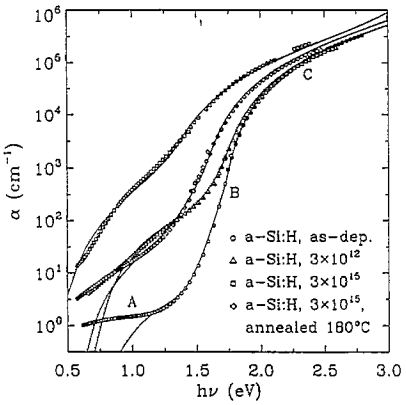


Fig. 3. Optical absorption spectra of a-Si:H after deposition, after implantation with 1 MeV $Si^+$ to doses of $3\times10^{12}$ and $3\times10^{15}$ ions $cm^{-2}$, and after post-implantation annealing at 180 °C.

Müller et al. [6]. From Fig. 3 it is clearly observed that the low-dose implantation already causes an increase in the defect-related absorption. The high-dose implant causes an extra absorption in region C, which could be modelled as owing to a decrease of the optical band gap of the material. Annealing causes both a decrease in the defect density and in the band gap. Qualitatively similar results were obtained for implanted unhydrogenated a-Si samples, although in the latter case the defect densities were approximately one order of magnitude higher than similarly treated a-Si:H samples. This difference demonstrates the well-known effect of passivation of point defects by hydrogen.

The effects of defect creation by ion implantation on various electrical, optical and structural properties of hydrogenated and unhydrogenated amorphous silicon are presented in Fig. 4. It is clear that damage accumulation owing to ion implantation dramatically affects the photocarrier lifetime, the average bond-angle variation and the optical band gap. Fig. 4(a) shows that the value of $\tau$ in a-Si:H decreases with ion dose and saturates at 2.5 ps. The slope of this decrease (close to unity) suggests that the density of electronic defects initially is proportional to the implantation dose. It is also noteworthy that for all ion doses the defect density in a-Si appears to be higher than in a-Si:H. The fact that the presence of hydrogen reduces the defect density is in agreement with optical absorption data and Raman studies, as can also be concluded from Fig. 4(b). Fig. 4(b) also indicates that ion irradiation increases the structural disorder in a-Si and a-Si:H in the same way. The optical gap data in Fig. 4(c) show a decrease of the gap for both types of materials and a saturation in the high-dose regime. For all implantation doses the value of $E_g$ in a-Si:H is 0.22 eV larger than in a-Si. Furthermore, the similarity between the S-shaped curves in the two lower figures suggests a strong correlation between structural disorder and band gap. The behaviour of the carrier lifetime versus ion dose is different. Here saturation sets in at a lower value of the ion dose. As a matter of fact, the saturation dose ($10^{14}$ $cm^{-2}$), is the same as found for the behaviour of dark conductivity of implanted a-Si:H samples (not shown).

The annealing behaviour of all of the mentioned properties has also been studied. Further details can be found in Ref. [1]. In this context, damage-saturated samples have a different annealing behaviour than low-dose implanted samples. It is generally observed that in samples implanted with high doses the global structural properties (band gap and bond-angle distribution) do not restore to their original (unimplanted) values. On the contrary, the density of single point defects, as measured by the carrier lifetime can, in many cases, be restored by annealing treatments. It was mentioned earlier that by modelling the optical absorption data, in combination with the measured carrier lifetimes, the value of $\tau$ can be related to the defect density. Also the width of the Raman TO peak can be related to the width of the bond-angle distribution. All these data now enable us to draw some interesting conclusions about the relation between point defect creation and bond-angle variation. These results are shown in Fig. 5, for the case of unhydrogenated a-Si. Starting from the relaxed state in the figure (bottom left), we observe that ion implantation raises the defect density from $1.7\times10^{19}$ to $4.5\times10^{19}$ $cm^{-3}$, while $\Delta\Theta$ remains at a constant level of 8.9°. Further irradiation results in a simultaneous increase in $N_{de}$ and $\Delta\Theta$, until $N_{de}$ reaches its saturation level of $2\times10^{20}$ $cm^{-3}$. Upon ion implantation $\Delta\Theta$ increases further from 10.2° to 11.0°, the value for fully damaged a-Si. Annealing

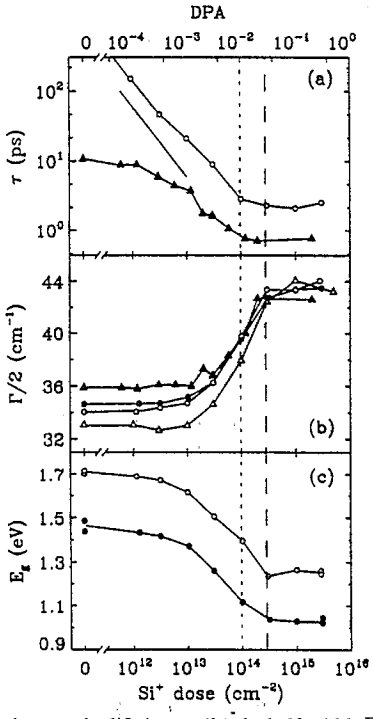


Fig. 4. (a) The photocarrier lifetime $\tau$, (b) the half-width $\Gamma/2$ of the Raman TO peak, and (c) the optical band gap $E_g$ as a function of 1 MeV $Si^+$ dose (bottom axis) and the number of displacements per atom DPA (top axis). The filled symbols refer to relaxed a-Si samples, prepared either by ion amorphization and annealing (triangles) or by dehydrogenation of a-Si:H (circles). Open symbold denote a-Si:H samples, deposited at 200 °C (circles) or 230 °C (triangles). The short-dashed and long-dashed lines represent the saturation doses for $\tau$, $\Gamma/2$, and $E_g$, respectively. The solid line in (a) represents a reciprocal relationship between $\tau$ and the ion dose.

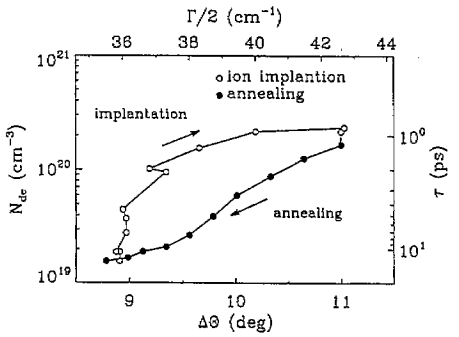


Fig. 5. The defect density $N_{de}$ (left axis) estimated from photocarrier lifetime measurements (right axis) versus the average bond-angle variation $\Delta\Theta$ (bottom axis) calculated from the Raman TO peak width $\Gamma/2$ (top axis) for a-Si. The open circles represent implanted samples, while the filled circles denote samples that were annealed after ion implantation.

of fully damaged a-Si results in a simultaneous reduction in $\Delta\Theta$ and $N_{dc}$, until the relaxed a-Si state is reached once again. These data suggest the following scenario for the accumulation of ion damage in a-Si. For low doses, small isolated damage clusters and point defects are formed in low concentrations. This leads to an increase in $N_{de}$ but without effect on $\Delta\Theta$. At higher damage levels, larger defect zones are formed. Finally, the properties are no longer affected by further irradiation because the additional produced defects recombine. It is interesting to note that $\Delta\Theta$ still increases where $N_{de}$ saturates. Similar results have been found for crystalline silicon [7], where it was also shown that the photocarrier lifetime in c-Si saturates far below the saturation threshold. Our results suggest that there is a limit to the density of defects which can be accommodated in the a-Si network. Fig. 5 clearly shows that the coupling between defects and the average bond-angle variation is different for implanted and annealed samples. We observe that, the structural disorder being the same, annealed samples have a smaller defect density. Apparently defects and bond-angle variation are separable to a large extent, which is an important modification to the general notion that the overall network strain in a-Si is entirely controlled by defects.

Similar results were obtained for a-Si:H. In this material, however, the beneficial influence of hydrogen on the network structure shows from a lower starting value of $\Delta\Theta$ and from the fact that the defect densities for comparable ion doses are an order of magnitude lower than in the case of a-Si. In this case, however, annealing cannot restore the original order, because of loss of hydrogen during the annealing treatments.

## 3. Ion beam synthesis of Er-doped optical gain materials

### 3.1. Soda lime silicate glass

In this section we will show recent experimental results on the ion beam synthesis of Er-doped optical waveguide materials operating at 1.5 $\mu$m. Er-doped waveguide amplifiers can be used, for example, to compensate for the losses in a Y-branch (1-to-2) splitter. In this case an optical gain of a factor 2 (3 dB) is required. To obtain such a gain in a waveguide of typically a few centimeters in length, Er concentrations of the order of 0.5 at.% are required. Soda-lime silicate glass has been doped with Er, using ion implantation. The advantage of this glass is that single-mode optical waveguides can be made using the relatively simple $Na^+$-$K^+$ ion exchange process from a $KNO_3$ melt. In this way, Na ions near the surface are replaced by K, thereby raising the refractive index in a typically 6 $\mu$m thick surface layer. Such waveguides are compatible with standard single mode silica fibers as far as the mode diameter and the refractive index are concerned.

Fig. 6 shows a photoluminescence spectrum of the Er-implanted silica glass (500 keV, $3.7\times10^{15}$ Er cm$^{-2}$) after annealing at 512 °C [8]. Annealing is necessary to remove implantation-induced defects which, by an interaction with the $Er^{3+}$ ions, reduce the luminescence lifetime and efficiency [9]. PL measurements are performed using an Ar ion laser at 514.5 nm as a pump source. This wavelength is resonantly absorbed at the $^2H_{11/2}$ manifold of the $Er^{3+}$ ion (see inset in Fig. 6). After rapid non-radiative relaxation to the $^4I_{13/2}$ level, the Er decays to the ground state by emission of a 1.54 $\mu$m photon. The spectrum in Fig. 6 is relatively broad owing to Stark splitting of the degenerate 4f levels in the electric field around the Er ion, as well as owing to inhomogeneous broadening as a result of the broad distribution of sites of Er in the multicomponent glass.

Fig. 7 shows PL lifetime measurements at 1.54 $\mu$m of Er in soda-lime glass as a function of Er peak concentration, measured after annealing at 512 °C [10]. The maximum concentration in Fig. 7 corresponds to a fluence of $1.8\times10^{16}$ Er cm$^{-2}$. As can be seen, a linear increase of the decay rate is observed. This effect is attributed to a concentration quenching effect: at high Er concentrations energy transfer can take place between an excited and an unexcited Er ion. This migration continues until a quenching center is met and the excitation is lost. This effect becomes stronger at higher

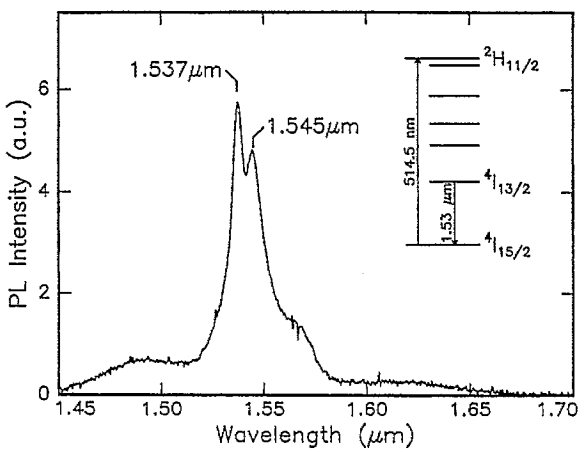


Fig. 6. Photoluminescence spectrum of Er-implanted soda-lime silicate glass (500 keV, $3.7\times10^{15}$ Er cm$^{-2}$) after thermal annealing at 512 °C for 1 h. The inset shows the energy level diagram of $Er^{3+}$.

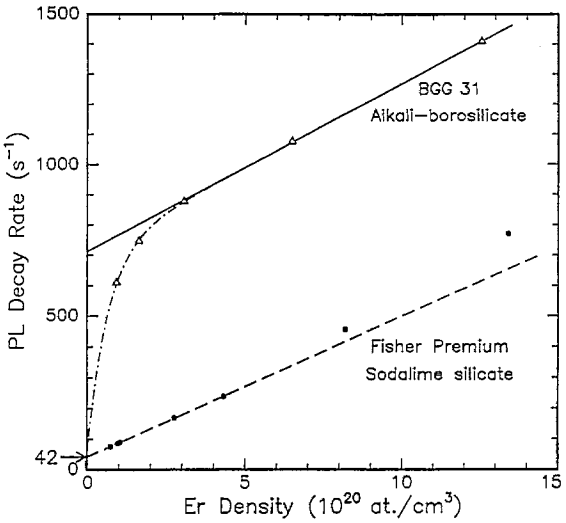


Fig. 7. Photoluminescence decay rate at 1.54 μm as a function of Er peak concentration for Er-implanted soda-lime silicate glass (500 keV, annealed at 512 °C) and borosilicate glass (400 keV, annealed at 400 °C). The lines are fits to the concentration quenching models discussed in the text.

Er concentration and results in an increase in the PL decay rate. In soda-lime glass, infrared absorption measurements have shown the presence of $8\times10^{18}$ OH $cm^{-3}$ [10]. OH groups are important quenching centers as the energy of the second harmonic of the OH stretch vibration corresponds to the 1.5 μm transition energy of $Er^{3+}$. In a simple concentration quenching model the PL decay rate $W_o$ as a function of Er concentration $N_{Er}$ is given by:

$$W_o = W_{rad} + W_i + C_{Er-Er}N_qN_{Er} \quad (1)$$

with $W_{rad}$ the radiative decay rate of Er, $W_i$ the internal non-radiative decay rate of each Er ion, and $N_q$ the density of quenching sites. The linear behaviour as a function of $N_{Er}$ predicted by Eq. 1 describes the data for sodalime glass in Fig. 7 quite well. The intercept at zero Er concentration found in Fig. 7 is 42 $s^{-1}$ (24 ms), close to the radiative decay rate $W_{rad}$ found in an independent experiment [11]. This implies that in Er-implanted sodalime glass $W_i = 0$, i.e. after thermal annealing no implantation-induced structural defects remain that couple directly to the Er.

Fig. 7 also shows data for 400 keV Er implanted alkali-borosilicate glass. This glass was annealed at 400 °C, the temperature at which the maximum PL intensity was obtained. For all Er concentrations the Er decay rate is much higher than for the sodalime glass. For concentrations above $3\times10^{20}$ Er $cm^{-2}$ the behaviour can be described by Eq. 1. Indeed, borosilicate glass contains OH quenching impurities, as determined by infrared absorption spectroscopy [10]. For low fluences a non-linear behaviour is found. This can be explained based on an assumption that in this glass radiation damage caused by the ion beam induces additional quenching of the Er by an increase of the internal quench rate $W_i$. The dash-dotted line through the data is based on a calculation [10] in which it is assumed that the damage coupling to the Er increases with Er fluence according to an overlap model, i.e. $W_i$ is proportional to $(1\text{-}\exp(-f/f_c))$ with $f_c$ a critical fluence. It is interesting to note that radiation damage is still present in this borosilicate glass even after annealing at 400 °C. This is consistent with earlier observations that the presence of B in the silica network results in rather stable radiation damage, owing to electronic energy loss processes [12]. The concentration quenching behaviour shown in Fig. 7 is a limitation for the application of these silicate glasses. For the typical Er concentrations required in an amplifier ($3\times10^{20}$ Er $cm^{-3}$) the PL lifetime is around 5 ms in sodalime glass and 1 ms in the borosilicate. These lifetimes are much lower than the purely radiative lifetimes of 24 ms. As a result, much higher pump powers are required to reach inversion in such Er-doped waveguides. A further disadvantage of these Na-K ion-exchanged waveguides is that the optical mode profiles are relatively wide (6–10 μm). Therefore, relatively high pump powers are required to reach high pump intensities in the Er-doped part of the waveguides.

### 3.2. *Erbium-doped hydrogenated amorphous silicon*

Another promising host material for Er is amorphous silicon. Being amorphous, it allows avoidance of the problem of limited solubility of Er in crystalline semiconductors, and to incorporate more of the impurities such as oxygen and carbon that are known to enhance the luminescence [13–15]. Earlier work on Er doping of pure amorphous Si has shown luminescence only at low temperature (77 K) [16]. More recent experiments have shown that room temperature photoluminescence [17] and electroluminescence [18] can be achieved from heavily oxygen-doped (30 at.%) amorphous Si (SIPOS). The disadvantage of this material is that its electrical quality is rather poor, and it is therefore interesting to investigate amorphous materials with better electrical quality.

Hydrogenated amorphous Si (a-Si:H) is a candidate material. Here we present a photoluminescence characterization of device-quality a-Si:H films doped with Er by ion implantation. These films show room-temperature 1.54 μm photoluminescence from $Er^{3+}$, with an intensity higher than what has been achieved in c-Si so far. A 250 nm thick a-Si:H film was deposited on glass (Corning 7059) by plasma enhanced chemical vapor deposition (PECVD) of $SiH_4$ at 230 °C. The H content in the films was 10 at.%, and a background concentration of 0.3 at.% O was also present, as measured by elastic recoil spectrometry. Erbium was implanted at 125 keV to a dose of $4\times10^{14}$ Er $cm^{-2}$, corresponding to a peak concentration of 0.2 at.%. In some samples, additional O was implanted at 25 keV to a dose of $7\times10^{15}$ O $cm^{-2}$, corresponding to a peak O concentration of 1.0 at.%, which overlaps with the Er profile. The Er doped samples with the two different O-contents refer to the low-O and high-O sample, respectively. After implantation, samples were annealed in a vacuum (base pressure $< 1\times10^{-6}$ mbar) for 2 h at various temperatures. Photoluminescence spectra were measured using the 515 nm line of an Ar laser as the excitation source

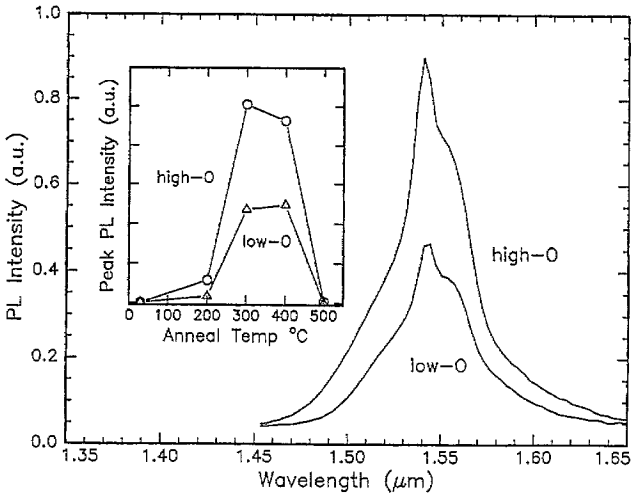


Fig. 8. Room temperature photoluminescence spectra of Er implanted a-Si:H with two different O contents: low O (0.3 at.%) and high-O (1.3 at.%). The Er fluence was $4\times10^{14}$ Er $cm^{-2}$ and both samples were annealed at 400 °C. The inset shows the peak intensity at 1.54 μm at room temperature as a function of the anneal temperature for both samples. All anneals were performed for 2 h. $\lambda_{pump}=515$ nm, pump power = 50 mW.

at a nominal power of 50 mW, and employing a mechanical chopper and standard lock-in techniques. All spectra were corrected for detection sensitivities.

Fig. 8 shows the room temperature photoluminescence spectra of Er-implanted a-Si:H samples (low-O and high-O), annealed at 400 °C, displaying characteristic $Er^{3+}$ luminescence at 1.54 mm. The inset shows the $Er^{3+}$ luminescence intensity at 1.54 μm as a function of the annealing temperature. As can be seen, samples annealed at 300–400 °C display the optimum $Er^{3+}$ luminescence. Therefore, these were chosen for all further studies. No erbium related luminescence can be observed from either the as-implanted samples nor from the samples annealed at 500 °C. The increasing and decreasing trends in the inset are attributed to the competing effects of removal of irradiation-induced defects and outdiffusion of hydrogen as the annealing temperature is increased. Hydrogen is essential for passivating the defects inherent in a-Si:H. It has been shown before that Er in pure a-Si without hydrogen does not luminesce at room temperature [16]. The room-temperature photoluminescence peak intensity for the high-O sample is more than two orders of magnitude larger than that for Er-implanted c-Si co-doped with oxygen and annealed for optimum luminescence, and measured under identical conditions.

Finally, it is interesting to discuss and compare the effect of O on the luminescence quenching in a-Si:H and c-Si. In general, O co-doping in c-Si can reduce the luminescence quenching, and this effect increases with O content [15]. For the highest O content studied in crystalline Si (0.2 at.%), the quench factor between 77 and 300 K was 30 [15]. However, in this case the absolute photoluminescence intensity was lower than for samples with lower O content, presumably owing to a reduction in minority carrier lifetime owing to the high O content. In contrast, in a-Si:H the O content can be increased to at least 1.3 at.% (high-O sample), causing a further increase in the photoluminescence intensity and a reduction in the quench factor to only a factor of 7, instead of 30. These data are shown in Ref. [19]. This shows the advantage of an amorphous host in accommodating large concentrations of impurities such as Er and O. Note that the Er-doped high-O sample in Fig. 8 showed two orders of magnitude more intensity than a comparable c-Si sample. This difference is partly ascribed to the higher optical absorption coefficient of a-Si, leading to higher carrier densities and hence higher excitation efficiency in the Er-implanted region.

## References

[1] A.J.M. Berntsen, *Thesis*, Utrecht, 1993.
[2] P. Stolk, *Thesis*, Utrecht, 1993.
[3] M.J. van den Boogaard, *Thesis*, Utrecht, 1992.
[4] G.D. Amer and W.B. Jackson, in J.I. Pankove (ed.), *Hydrogenated Amorphous Silicon*, Academic Press, Orlando, 1984, p. 329.
[5] G. Lucovsky, *J. Non-Cryst. Solids, 76* (1985) 173.
[6] G. Müller, H. Mannsperger and S. Kalbitzer, *Philos. Mag., B53* (1986) 257.
[7] P.A. Stolk, L. Calcagnile, S. Roorda, H.B. van Linden van den Heuvell and F.W. Saris, in G. Was, L.E. Rehn and D. Follstaedt (eds.), *Phase Formation and Modification by Beam-Solid Interactions*, Materials Research Society, Pittsburgh, 1992, p.15.
[8] E. Snoeks, G.N. van den Hoven and A. Polman, *J. Appl. Phys., 75* (1994) 2644.
[9] A. Polman and J.M. Poate, *J. Appl. Phys., 73* (1993) 1669.
[10] E. Snoeks, P. Kik and A. Polman, *Opt. Mater., 5* (1996) 159.
[11] E. Snoeks, A. Lagendijk and A. Polman, *Phys. Rev. Lett., 74* (1995) 2450.
[12] D.L. Griscom, G.N. Sigel Jr. and R.J. Ginther, *J. Appl. Phys., 47* (1976) 960.
[13] J. Michel, J.L. Benton, R.F. Ferrante, D.C. Jacobson, D.J. Eaglesham, E. A. Fitzgerald, Y.H. Xie, J.M. Poate and L.C. Kimerling, *J. Appl. Phys., 70* (1991) 2672.
[14] S. Coffa, G. Franz, F. Priolo S, A. Polman and R. Serna, *Phys. Rev. B,* (1994) 16313.
[15] F. Priolo, G. Franz, S. Coffa, A. Polman and S. Libertino, R. Barklie and D. Carey, *J. Appl. Phys., 78,* (1995) 3874.
[16] J. S. Custer, E. Snoeks and A. Polman, *Mater. Res. Soc. Symp. Proc., 235* (1992) 51.
[17] G.N. van den Hoven, Jung H. Shin, A. Polman, S. Lombardo and S.U. Campisano, *J. Appl. Phys., 78* (1995) 2642.
[18] S. Lombardo and S. U. Campisano, G. N. van den Hoven and A. Polman, *J. Appl. Phys., 77* (1995) 6504.
[19] J.H. Shin, R. Serna, G.N. van den Hoven, A. Polman, W.G.J.H.M. van Sark and A.M. Vredenberg, *Appl. Phys. Lett., 68* (1996) 997.